Orientation Sensitive SEIRA Sensors based on

Single-Walled Carbon Nanotube Near Fields

Kyriacos Georgiou, 1,2† Yulei Wang, 1,2 Xuedan Ma^{1,2,3*}

¹Center for Nanoscale Materials, Argonne National Laboratory, Lemont, Illinois 60439, United

States

²Consortium for Advanced Science and Engineering, University of Chicago, Chicago, Illinois

60637, United States

³Department of Materials Science and NanoEngineering, Rice University, Houston, Texas

77005, United States

*Email: xuedan.ma@rice.edu

Abstract

Molecular vibrations that bear information about intrinsic properties of chemical compounds are

challenging to detect at sub-monolayer densities. Surface-enhanced infrared absorption (SEIRA)

spectroscopy has been proven to be a viable approach to enhance and detect weak vibration signals.

Here, we report a SEIRA sensor based on mid-infrared surface plasmon resonances supported by

single-walled carbon nanotubes (SWCNTs). Due to the 1D nature of SWCNTs, their plasmon

1

modes are highly polarized with the electromagnetic fields spatially confined to nanometer scales. Leveraging these characteristics of SWCNTs, we observe a polarization selective coupling between their surface plasmons and vibrational modes of chemical bonds introduced to their surfaces. A maximum modulation of ~ 15% to the plasmon resonance peak is obtained for a submonolayer chemical group coverage density. These findings suggest that SWCNTs may potentially serve as a highly sensitive SEIRA platform for revealing intricate information about molecular compositions and bond orientations.

KEYWORDS: infrared absorption, surface plasmon, carbon nanotube grating, molecular vibration, SEIRA sensor, Fano resonance

Infrared spectroscopy probing molecular vibrations at mid-infrared (IR) wavelengths could reveal valuable information about the molecules' compositions, chemical bonds, and configurations. ¹ It therefore serves as a nondestructive label-free detection method for identifying molecular species and chemical compounds. However, in dilute systems where the analyte density is well below monolayer coverage, this detection method becomes challenging. This is due to the several orders of magnitude mismatch between mid-IR wavelengths and typical molecule dimensions, ^{2, 3} that render the absorption cross section of molecular vibrations inherently small (typically on the order of 10^{-20} cm²), ⁴ a crucial factor hampering the probe of minute amounts of analytes as is often required in sensing applications. One possibility to overcome this limitation is to improve the sensitivities of IR detectors. ⁵⁻⁷ Another strategy relies on enhancing IR light - vibration interaction

based on the Fermi's golden rule,^{8, 9} that is in the weak coupling regime, the ground-to-excited state transition rate is proportional to the local electric field intensity. Using strong near fields confined in the vicinities of photonic nanostructures, surface-enhanced infrared absorption (SEIRA) has demonstrated to improve the detection sensitivity of molecular vibrations profoundly.^{3, 10}

Among the various types of IR plasmonic materials explored for SEIRA applications, carbon nanostructures such as single-walled carbon nanotubes (SWCNTs) offer several unique features. Surface plasmons in SWCNTs arise from longitudinal electronic oscillations and can be reflected in Fabry-Pérot like resonators formed by the nanotube ends (Figure 1a). 11-13 Compared to photonic resonators fabricated from bulk films and graphene nanoribbons, surface plasmons in SWCNTs offer strong one-dimensional field confinement, tube length-dependent broadband surface plasmon resonances, and the possibility for post-fabrication tuning via electrostatic gating. The high mechanical stability of SWCNTs also renders them highly compatible with flexible electronic devices.

Despite these appealing characteristics of surface plasmons in SWCNTs, applying them in SEIRA sensors was largely hampered due to the requirement of wafer-scale high-density well-aligned SWCNT arrays. In recent years, methods for the preparation of aligned SWCNT films have been further optimized, mainly driven by their needs in electronic devices. ¹⁴ These approaches include Langmuir-Schaefer deposition, ¹⁵ evaporative self-assembly, ^{16, 17} and vacuum filtration ^{18, 19} among others. In particular, the slow vacuum filtration technique reported by He et al. ¹⁸ has been shown to afford large-area, globally-aligned monodomain SWCNT films with controllable thicknesses. Recent efforts in using automated and parallelized filtration setups that allow in situ measurements of film formation suggest the possibility for reproducible and scalable production of such films. ^{19,}

²⁰ These advances in thin film preparation methods open the door to SWCNT surface plasmon-based SEIRA sensors.^{13, 21}

Here, we report that SWCNT arrays have the potential to realize high-performance SEIRA sensors due to their strongly confined 1D electromagnetic fields in the mid-IR range. As a proof-ofconcept, we create surface plasmon resonators based on aligned SWCNT arrays patterned into gratings and study their interactions with nitrobenzene groups that are covalently bonded to their surfaces. When the plasmon modes are tuned into resonance with the vibrational energy of C-H bonds (~ 1245 cm⁻¹) in the nitrobenzene functional groups, we find a nearly 15% modulation of the resonators' reflection spectrum for an estimated coverage density of a few hundred nitrobenzene groups/µm², a value that is much smaller than a monolayer coverage density based on our estimations. Moreover, in contrast to the strong modulations caused by the weak C-H bonds whose dipoles align with the plasmon electric fields, the absence of modulations associated with the strong N=O bonds whose dipoles lie perpendicularly to the electric fields suggests that the plasmon resonances in SWCNTs can reveal molecular orientation information. These findings highlight the unique characteristics of surface plasmons in SWCNTs and their potential for highly sensitive SEIRA sensors for probing and identifying trace amounts of chemical compounds that would otherwise be challenging with conventional spectroscopic techniques.

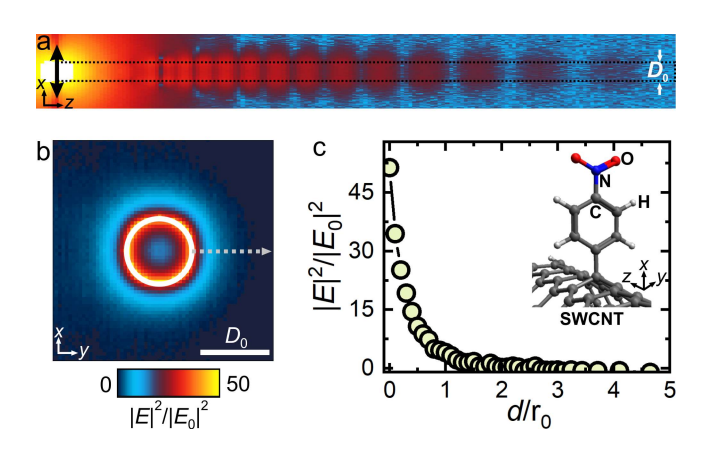


Figure 1. (a) Simulated spatial distributions of the vertical component of the electric field, $|E_z|$, close to a SWCNT with a diameter of D_0 (indicated by dashed lines). A point dipole (indicated by the arrow) separated 0.5 nm from the SWCNT end is used to launch the surface plasmon. (b) Local electric field enhancement distributions, $|E|^2/|E_0|^2$, in the vicinity of a SWCNT. The diameter of the SWCNT, D_0 , is used as the scale bar. (c) Changes in the enhancement factor $|E|^2/|E_0|^2$ as the distance, d, from the SWCNT surface increases. The data correspond to the dashed line in (b). Inset: schematic of the nitrobenzene functional group on the surface of a SWCNT.

In order to optimize the coupling between surface plasmon resonators and molecular vibrations, the system needs to meet two necessary conditions: i) the chemical bonds hosting the vibrational modes should spatially overlap with the electromagnetic fields confined by the surface plasmon resonators, and ii) the plasmonic and vibrational modes are degenerate in energy. To meet the first requirement and understand local electromagnetic fields confined by SWCNT resonators, we start by performing numerical simulations of their plasmon resonances (see Methods in the Supporting Information for simulation details). The dielectric constant of the SWCNTs is described by a standard Drude model which has been demonstrated to give reasonable estimations for their optical properties. 12, 22, 23 Figure 1b-1c shows the local electric field distributions of the plasmon resonances, which are highly confined to the SWCNT surfaces with their intensities decreasing monotonically as the distance from the SWCNT surfaces increases. From the simulated distributions of electric fields, we estimate that $\sim 90\%$ of the resonance energy is confined within ~ 5 nm from the SWCNT surface. Due to the 1D nature of SWCNTs, the confinement of these plasmon modes could be much stronger than those in metal-based photonic resonators, although it also indicates that close distances between the analytes and SWCNT surfaces would be required to fully leverage the strongly confined near-fields. To achieve maximum coupling between the surface plasmon resonances and vibrational modes, we introduce functional groups, namely nitrobenzene (Figure 1c inset), onto SWCNT surfaces through a controlled functionalization approach.^{24, 25} Given the sensitivity window of our Fourier transform infrared (FT-IR) setup (Figure S1), we choose to focus on the IR fingerprint region between 1100 – 1400 cm⁻¹. This energy range covers the key vibrational modes in the nitrobenzene functional groups: the weakly absorbing C-H bending modes at ~ 1160 cm⁻¹ and 1245 cm⁻¹, the C-C stretching mode in the benzene ring at 1310 cm⁻¹, and the strongly absorbing N=O stretching mode at 1350 cm⁻¹ (see Figure S2 for the complete FT-IR spectrum of nitrobenzene).^{26, 27} These modes are within 1 nm distance from the SWCNT surface, well in the region where strong field enhancement is expected.

Due to the Fabry-Pérot nature of surface plasmons in SWCNTs, their resonance energies can be tuned by adjusting the tube lengths. To achieve this, we first prepare SWCNT films using the slow vacuum filtration method that allows the formation of well-aligned films with thicknesses in the range of a few tens of nanometers (Figure 2a, see Methods in the Supporting Information for details). An image of a representative dried polycarbonate filter membrane is shown in Figure 2b where the aligned SWCNT 'cake' appears as a dark area in the central region of the filter. The process was repeated for dispersion of SWCNTs that were functionalized with nitrobenzene groups using a controlled functionalization method. Specifically, to decorate the SWCNTs with a nitrobenzene functional group, we added 20 μ L of 0.8 mg/mL 4-nitrobenzenediazonium tetrafluoroborate in acetonitrile into 500 μ L of 80 μ g/mL SWCNTs in 0.25% sodium dodecyl sulfate (SDS)/DI-water, and stirred the mixture for 45 minutes under ambient conditions. Once designated defect densities were achieved as determined by Raman spectroscopy (vide infra), the reaction was stopped by adding 1% SDS/DI-water to the solution. To be used for the slow vacuum

filtration, the solution was further diluted by DI-water to achieve a final concentration of 8 μ g/mL SWCNT in 0.1% SDS/DI water.

In order to quantify the degree of alignment of the SWCNTs, the as-prepared films were characterized using polarization-dependent Raman spectroscopy as shown in Figure 2d-2e. Maximum Raman signals can be detected when the laser excitation and scattering detection polarizations are parallel to the alignment direction of the carbon nanotubes (I_{HH}), while for a configuration where both polarizations are perpendicularly aligned to the nanotubes (I_{VV}), the Raman signal is suppressed. These polarization-dependent Raman measurements of both pristine and functionalized films reveal that the films are highly aligned with an estimated nematic order parameter (S_{Raman}) greater than 0.9. Note that we have observed a slightly smaller S_{Raman} in functionalized SWCNT films. We speculate that this is a result of the presence of small amounts of acetonitrile and potentially other chemical by-products in the functionalized dispersion that could affect the SWCNTs' local environment and consequently the alignment process during the slow vacuum filtration. In addition, changes in the surface morphologies of the SWCNTs following the functionalization with nitrobenzene groups may also influence the inter-tube interactions and stacking process.

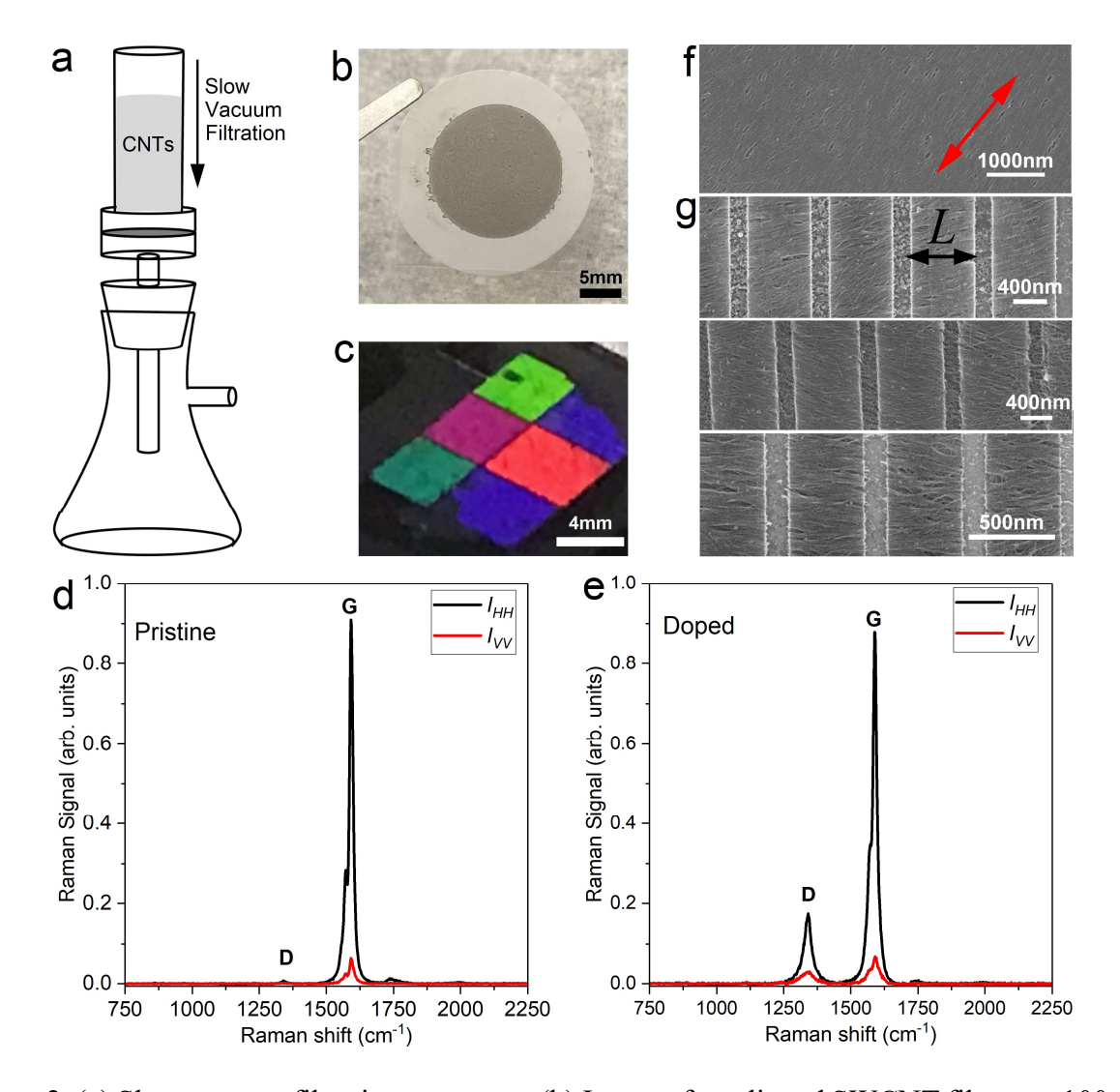


Figure 2. (a) Slow vacuum filtration apparatus. (b) Image of an aligned SWCNT film on a 100 nm-porous polycarbonate filter following a slow vacuum filtration. (c) Diffraction of white light on an etched SWCNT sample where the different colors indicate diffractions of light on SWCNT gratings with different pitches. (d, e) Polarized Raman spectra of (d) pristine and (e) diazonium functionalized SWCNT films, obtained when the linearly polarized laser excitation is either parallelly (I_{HH} , black solid line) or perpendicularly (I_{VV} , red solid line) aligned with respect to the SWCNT orientation. (f) SEM image of an aligned SWCNT film after having been transferred onto a polished Si substrate. The red arrow indicates the direction of the global alignment. (g) SEM images of aligned SWCNT gratings with different pitches.

Raman spectroscopy also reveals information about the functional group coverage on the SWCNT surfaces. Pristine samples (Figure 2d) show an intense G-band at 1591 cm⁻¹, with the characteristic defect-related D-band at 1341 cm⁻¹ being largely negligible ($I_D/I_G \sim 0.5\%$). On the other hand, Figure 2e shows the Raman signal of a sample that has been functionalized with the nitrobenzene groups. Here it is clear that apart from the expected G-band, a D-band with a notable intensity has emerged ($I_D/I_G \sim 30\%$), which can be attributed to the nitrobenzene groups introduced onto the surfaces of the SWCNTs. Based on the intensity ratio between the D- and G-bands, we estimate the functional group density to be ~ 20 nitrobenzene groups per a 1 µm long tube. ^{28, 29} We would like to note that the SWCNT samples used in this study consist of both metallic and semiconducting nanotubes (see Figure S3 for its absorption spectrum), and the coverage density derived from the Raman signatures is likely an underestimation for the following reasons: a) the 532 nm excitation wavelength used in the Raman measurements is more efficient in exciting the semiconducting nanotubes than the metallic ones used in this study.³⁰ Therefore, the Raman spectra primarily capture defect densities in the semiconducting nanotubes, but not the metallic ones. b) Metallic nanotubes have been shown to be more reactive than the semiconducting ones during similar diazonium functionalization reactions.³¹ Despite these factors that make accurate quantifications of defect densities challenging, we expect that the values provided here to be reasonable estimations.

To fabricate SWCNT-based plasmon resonators, their aligned films were attached face-down onto high resistivity float zone silicon substrates, with the polycarbonate filters being dissolved using a chloroform bath (see Methods in the Supporting Information for details). Scanning electron microscopy (SEM) was used to image the surfaces of the transferred films as shown in Figure 2f, with the red arrow indicating the alignment orientation. Next, to pattern the aligned SWCNTs into

gratings of specific lengths, the films were coated with a positive e-beam resist, and e-beam lithography was utilized to write grating-like patterns onto the films. The length (L) of the designed SWCNT ribbons ranged between 300 nm and 900 nm, with the spacing between the ribbons being maintained at a fixed length of 150 nm, similar to previous reports. Reactive ion etching (RIE) was used to etch down the resist-developed areas. Typical SEM images of patterned samples are shown in Figure 2g for a number of gratings with different pitches. An image of white light being diffracted from the different etched regions is shown in Figure 2c with the different colors resulting from grating-like patterns comprised of different SWCNT lengths and consequently grating pitches.

We use FT-IR spectroscopy to characterize the surface plasmon resonances supported by the different SWCNT gratings. A wire-grid mid-infrared polarizer was used in the setup to control the polarization of the incident infrared beam. All the FT-IR experiments discussed below were performed using an IR light with a linear polarization parallel to the orientation of the SWCNT alignment. The IR beam diameter is estimated to be < 1 mm. Figure 3a shows a series of measurements for pristine SWCNT samples having an L ranging from 300 nm to 900 nm and a measured film thickness of t = 57 nm. As can be seen in the figure, there appears to be an absorption peak for each sample corresponding to a surface plasmon resonance, with its energy dependent on the ribbon length L. We would like to note that the sharp dip at ~ 1262 cm⁻¹ is caused by background and likely associated with the IR lamp or the detection environment, rather than specific features from the SWCNT ribbons (see Figure S1 for background IR spectra).

The energy of the plasmon resonance (v_p) is correlated with the length L of the SWCNT ribbons and decreases as L increases, as expected from the linear relationship between plasmon frequency

and wavevector (q), $v_p \propto \sqrt{q}$, where $q = \pi/L$.²¹ The dashed line in Figure 3b represents the theoretically calculated energies of plasmon resonances as a function of SWCNT ribbon length, L, for a 57 nm thick film (see Figure S4 for calculated plasmon resonance energies of gratings with different thicknesses, t, and length, L). Together shown are the experimental peak absorption energies of the plasmon resonances (Figure 3b, dots). To extract this information from the FT-IR spectra, we fit the plasmon resonance peaks with Lorentzian functions (see Figure S5a for fitting results). Note that in the theoretical calculations, we assume a perfectly smooth film with a uniform thickness t over the entire IR irradiation area. Additionally, the plasmon energies are calculated for the case where the SWCNT ribbons are perfectly perpendicular to the direction of the gratings. In practice, misalignment between the SWCNTs and grating orientations has shown to cause shifts in the plasmon energy.³² We believe that factors such as variations in the film thickness over the detection areas and misalignment in the SWCNT-grating orientations could have led to the small discrepancies observed between the theoretical and experimental values in Figure 3b. Samples with smaller L values are even more prone to energy discrepancies because, apart from the aforementioned factors, they possess higher sensitivity to small fluctuations in the ribbon length L (i.e. larger $\Delta L/L$) that could shift the plasmon energies substantially.

The peak energy (v_p) and full width at half-maximum (Δv_p) of the plasmon resonances extracted from the Lorentz fits are used to estimate Q factors $(v_p/\Delta v_p)$ for each L measured, as is illustrated in Figure 3c (dots). As a guide to the eye, we have overlaid the experimental data with an exponential decay curve (dashed line). The Q-factor values range between 1 and 2 and drop with an increasing L, an observation that has been reported before in similar systems.²¹ Here, misalignment between the grating and SWCNT orientations is expected to affect the Q-factors of

the system due to an averaging effect over the measured area that causes linewidth broadening of the surface plasmon modes.

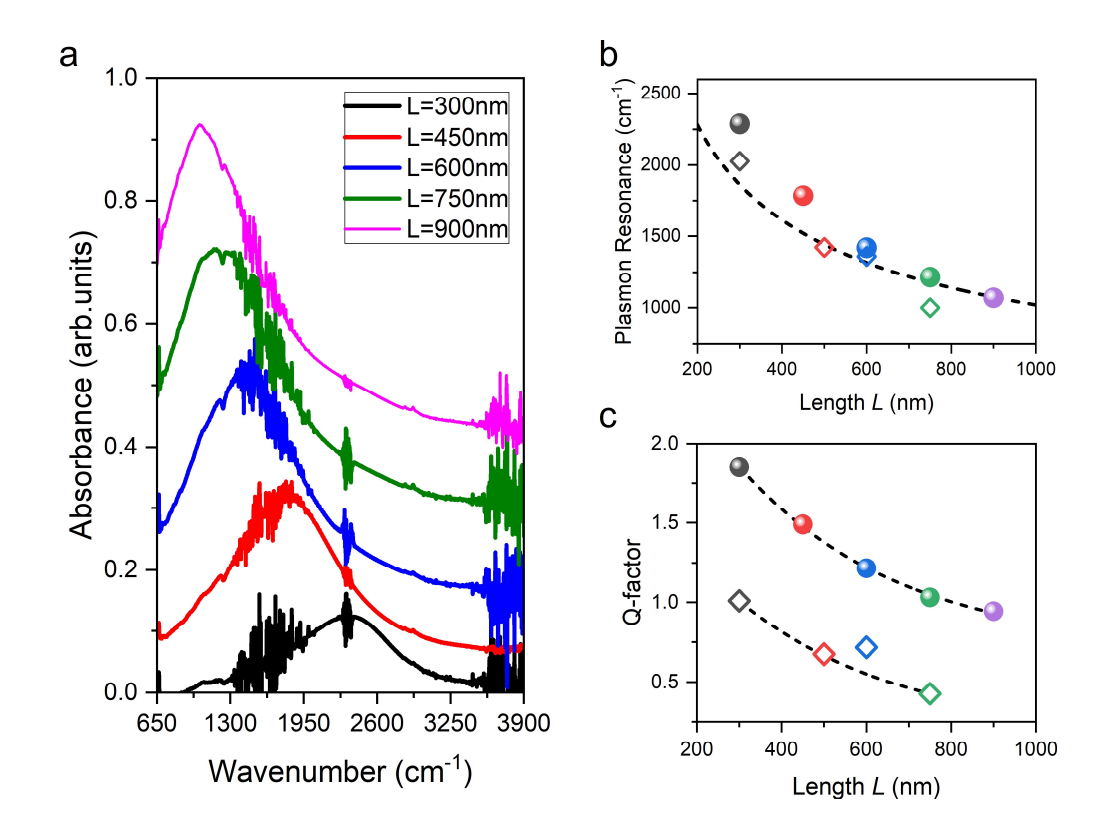


Figure 3. (a) FT-IR spectra of patterned pristine SWCNT gratings with different L values. For clarity, the spectra are vertically offset. (b) Calculated plasmon resonance energies as a function of tube length, L, for a 57 nm thick film (dashed lines), along with the peak absorption wavenumbers of the plasmon resonances extracted from the FT-IR spectra: dots correspond to pristine SWCNT gratings, and diamonds to functionalized SWCNT gratings. (c) Calculated Q-factors as a function of L, with dots representing pristine SWCNT gratings and diamonds functionalized SWCNT gratings. The black dashed lines are guides to the eye.

After having established surface plasmon resonances supported by SWCNT gratings, we continue to investigate their coupling with the nitrobenzene groups on SWCNT surfaces. To unveil any potential coupling effects between the vibrational modes in the nitrobenzene groups and SWCNT

surface plasmons, we utilize the functionalized SWCNTs to prepare gratings supporting plasmon resonances spanning the energy of $1000 - 2000 \text{ cm}^{-1}$. Figure 4a shows FT-IR measurements of functionalized SWCNT samples with L values varying between 300 nm and 750 nm and a measured film thickness of t = 57 nm. Consistent with those fabricated from pristine SWCNTs, the functionalized SWCNT gratings show the characteristic energy shifts for different L values (Figure 3b, diamonds; see Figure S5b for Lorentz fits). Their Q-factor values also show the expected reduction with an increasing L value (Figure 3c, diamonds). However, their spanning range suffers a two-fold decrease as compared to the pristine case. This is likely a result of the increased inhomogeneous alignment seen in functionalized SWCNT films (vide supra). Another potential reason could be that the covalent functionalization reduces local structural integrities of the SWCNT backbones, hence reducing their surface plasmon qualities.

Interestingly, superimposed on the broad plasmon resonance peaks, there are sharp attenuation features at the wavenumbers of ~1245 and 1310 cm⁻¹, which overlap well with the in-plane C-H bending mode (Figure 4b, red) and the C-C stretching mode in the benzene ring (Figure 4b, yellow), respectively. Intensities of these attenuation features gradually increase and peak when they become resonant with the plasmon resonance energy (indicated by the gray region in Figure 4a). The maximum visibility of the 1245 cm⁻¹ feature is achieved for a ribbon length of L = 600 nm, whose plasmon resonance mode is nearly on resonance with the sharp feature. Moreover, the line shapes of the sharp features become highly asymmetric as they approach the plasmon resonance, and can be well described using the Breit-Wigner-Fano function³³ (see Figure 4c for fitting results): $I(\omega) \propto \frac{[1+(\omega-\omega_0)/q\Gamma]^2}{1+[(\omega-\omega_0)/\Gamma]^2}$, with q being the Fano parameter representing the interactions of vibrational modes with surface plasmon resonances, and Γ the linewidth. This kind

of Fano resonance is characteristic of interferences between a discrete quantum state with a continuum band of states. Based on these observations, we assign the sharp features to C-H bending and C-C ring stretching modes-induced transparency, a manifestation of SEIRA due to the presence of the SWCNT plasmon resonance. We also estimate that a sub-monolayer C-H bending mode coverage density could lead to a $\sim 15\%$ modulation to the plasmon resonance peak. We would like to note that these parameters are bound by the sensitivity of the detectors as they are derived from measurements of grating arrays in a ~ 1 mm diameter area, which allow us to obtain sufficient signal-to-noise ratio in the FT-IR measurements.

Another notable observation is the absence of modulation caused by the much stronger N=O stretching mode at 1350 cm⁻¹ (Figure 4b). This seemingly strange finding reflects the unique characteristics of plasmon resonances in SWCNTs. Due to the 1D nature of SWCNTs, the electric fields of their surface plasmon resonances are predominantly oriented along the tube axis, namely the E_z orientation in Figure 1a-1b. Since the in-plane C-H bending mode in the nitrobenzene group at ~1245 cm⁻¹ has a dipole component parallel to the SWCNT surface (same for the C-C ring stretching mode at 1310 cm⁻¹), ^{26, 34} its dipole orientation can align well with the surface plasmon electric field (Figure 4b, top left), leading to efficient coupling between the C-H bending mode and the plasmon resonance. In contrast, the N=O stretching mode (so is the C-H bending mode at ~ 1160 cm⁻¹) has a dipole that is predominantly perpendicular to the SWCNT surface^{26, 34} (Figure 4b, top right) and consequently, its plasmon resonance electric field. As a result, the coupling of the N=O stretching mode with the surface plasmon resonances in the SWCNTs is negligible and despite the much stronger intensity of the N=O stretching mode, its signature is absent in the FT-IR spectra of the functionalized SWCNT gratings. This dipole orientation-dependent coupling is unique to the 1D surface plasmon modes in SWCNTs and can reveal intricate orientational

information of analytes, although in order to derive this information, the relative orientations of the analytes on the SWCNT surface should be fixated during the measurements. Another potential factor that may contribute to the modulation differences between the N=O stretching mode and the C-H bending mode is that the former is slightly farther away from the SWCNT surface (by ~ 2 - 3 Å), hence experiences a weaker field intensity. However, based on the distance-dependent field reduction rate in Fig. 1b - c and the relative absorption intensity ratio between the N=O stretching mode and the C-H bending mode in Fig. 4b (orange curve), we exclude the different field intensities experienced by the two vibrational modes to be the main reason, if at all, for the absence of modulation caused by the N=O mode. Overall, we conclude that carefully designed SWCNT plasmon resonators have the potential to serve as highly sensitive SEIRA sensors for probing weakly absorbing molecular vibrations.

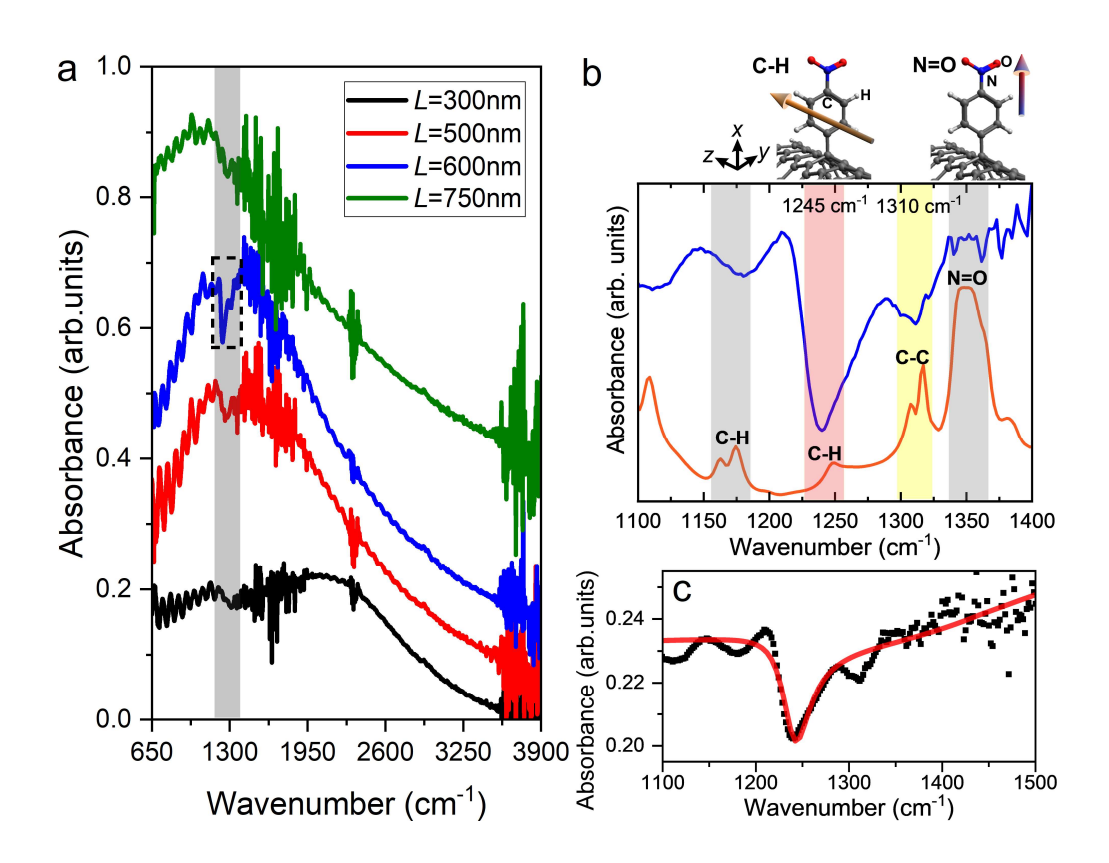


Figure 4. (a) FT-IR spectra of functionalized SWCNT gratings with different L values. The gray region indicates the energies of the IR features caused by the nitrobenzene group. For clarity, the spectra are vertically offset. (b) Bottom: A zoomed view of the section in the dashed rectangle in (a) (blue), together with the IR absorption spectrum of nitrobenzene (orange). Top: dipole orientations of the C-H bending mode at ~1245 cm⁻¹ and N=O stretching mode at 1350 cm⁻¹, with respect to the SWCNT surfaces. (c) A zoomed view of the section in the dashed rectangle in (a). The red curve represents a Breit-Wigner-Fano function fit, with $\omega_0 = 1240$ cm⁻¹, q = 4.9, and $\Gamma = 17.6$ cm⁻¹, respectively.

In summary, we use the slow vacuum filtration technique to prepare aligned SWCNT films and fabricate grating-like patterns that support surface plasmon resonances whose energies can be controlled by varying the grating pitch. Using the C-H bending mode in nitrobenzene as an example, we demonstrate that surface plasmon resonances in SWCNTs can interact efficiently with molecular vibrations in their vicinity, leading to apparent modulations to their plasmon resonance profiles. These findings suggest that SWCNT-based plasmon resonators have the potential to serve as SEIRA sensors for the detection of small traces of molecular compounds by leveraging highly confined near fields. Given the potential high sensitivity of this system, its sensing applications could be suitable for in situ monitoring by exposing the SWCNT resonators to the analytes' native environments. A potential advantage of SWCNT-based SEIRA sensors is the possibility of using electrostatic gating to adjust their plasmon resonances, 35, 36 so that their energies could be tuned into resonance with analyte vibrational modes. These characteristics make SWCNT-based plasmon resonators relevant for highly sensitive SEIRA applications, which we believe is achievable through further improvements in the film and grating qualities.

ASSOCIATED CONTENT

Supporting Information. The following files are available free of charge.

Experimental methods; Reference FT-IR spectrum; FT-IR spectrum of nitrobenzene; absorption

spectra of the SWCNTs; calculated plasmon resonance energies as a function of film thickness

and ribbon length; FT-IR spectra of patterned pristine and functionalized SWCNT films together

with the Lorentz fits.

AUTHOR INFORMATION

Present Addresses

†Department of Physics, Laboratory of Ultrafast Science, University of Cyprus, Nicosia 1678,

Cyprus.

Notes

The authors declare no competing financial interest.

ACKNOWLEDGMENT

17

We acknowledge support from the National Science Foundation CBET Program under award no. 2025214. Work performed at the Center for Nanoscale Materials, a U.S. Department of Energy Office of Science User Facility, was supported by the U.S. DOE, Office of Basic Energy Sciences, under Contract No. DE-AC02-06CH11357. X.M. acknowledges support from the startup grant from Rice University.

REFERENCES

- 1. Chalmers, J. M.; Griffiths, P. R. *Handbook of Vibrational Spectroscopy*. John Wiley & Sons **2002**.
- 2. Rodrigo, D.; Limaj, O.; Janner, D.; Etezadi, D.; Javier García de Abajo, F.; Pruneri, V.; Altug, H. *Mid-infrared plasmonic biosensing with graphene*. *Science* **349**, 165-168 (2015).
- 3. Yang, X.; Sun, Z.; Low, T.; Hu, H.; Guo, X.; Javier García de Abajo, F.; Avouris, P.; Dai, Q. *Nanomaterial-Based Plasmon-Enhanced Infrared Spectroscopy*. *Adv. Mater.* **30**, 1704896 (2018).
- 4. Huffman, D. R.; Bohren, C. F. *Absorption and Scattering of Light by Small Particles*. WILEY-VCH Verlag GmbH & Co. KGaA **1998**.
- 5. Tan, C. L.; Mohseni, H. *Emerging technologies for high performance infrared detectors. Nanophotonics* **7**, 169-197 (2017).
- 6. Tang, X.; Ackerman, M. M.; Chen, M.; Guyot-Sionnest, P. *Dual-band infrared imaging using stacked colloidal quantum dot photodiodes*. *Nat. Photon.* **13**, 277-282 (2019).
- 7. Li, X.; Nie, W.; Ma, X. Intersubband Transitions in Lead Halide Perovskite-Based Quantum Wells for Mid-Infrared Detectors. J. Phys. Chem. Lett. 14, 4766-4774 (2023).
- 8. Novotny, L.; Hecht, B. Principles of nano-optics. Cambridge University Press 2012.
- 9. Peng, L.; Wang, X.; Coropceanu, I.; Martinson, A. B.; Wang, H.; Talapin, D. V.; Ma, X. *Titanium Nitride Modified Photoluminescence from Single Semiconductor Nanoplatelets*. *Adv. Funct. Mater.* **30**, 1904179 (2019).
- 10. Neubrech, F.; Huck, C.; Weber, K.; Pucci, A.; Giessen, H. Surface-Enhanced Infrared Spectroscopy Using Resonant Nanoantennas. Chem. Rev. 117, 5110-5145 (2017).
- 11. Morimoto, T.; Joung, S.-K.; Saito, T.; Futaba, D. N.; Hata, K.; Okazaki, T. *Length-Dependent Plasmon Resonance in Single-Walled Carbon Nanotubes*. *ACS Nano* **8**, 9897-9904 (2014).
- 12. Lamata, I. S.; Alonso-González, P.; Hillenbrand, R.; Nikitin, A. Y. *Plasmons in Cylindrical 2D Materials as a Platform for Nanophotonic Circuits. ACS Photon.* **2**, 280-286 (2015).
- 13. Falk, A. L.; Chiu, K.-C.; Farmer, D. B.; Cao, Q.; Tersoff, J.; Lee, Y.-H.; Avouris, P.; Han, S.-J. Coherent Plasmon and Phonon-Plasmon Resonances in Carbon Nanotubes. Phys. Rev. Lett. 118, 257401 (2017).

- 14. He, M.; Zhang, S.; Zhang, J. Horizontal Single-Walled Carbon Nanotube Arrays: Controlled Synthesis, Characterizations, and Applications. Chem. Rev. 120, 12592–12684 (2020).
- 15. Cao, Q.; Han, S.-J.; Tulevski, G. S.; Zhu, Y.; Lu, D. D.; Haensch, W. *Arrays of single-walled carbon nanotubes with full surface coverage for high-performance electronics. Nat. Nanotechnol.* **8**, 180-186 (2013).
- 16. Jinkins, K. R.; Foradori, S. M.; Saraswat, V.; Jacobberger, R. M.; Dwyer, J. H.; Gopalan, P.; Berson, A.; Arnold, M. S. *Aligned 2D carbon nanotube liquid crystals for wafer-scale electronics*. *Sci. Adv.* 7, eabh0640 (2024).
- 17. Li, H.; Hain, T. C.; Muzha, A.; Schöppler, F.; Hertel, T. Dynamical Contact Line Pinning and Zipping during Carbon Nanotube Coffee Stain Formation. ACS Nano 8, 6417–6424 (2014).
- 18. He, X.; Gao, W.; Xie, L.; Li, B.; Zhang, Q.; Lei, S.; Robinson, J. M.; Hároz, E. H.; Doorn, S. K.; Wang, W.; Vajtai, R.; Ajayan, P. M.; Wade Adams, W.; Hauge, R. H.; Kono, J. *Wafer-scale monodomain films of spontaneously aligned single-walled carbon nanotubes*. *Nat. Nanotechnol.* 11, 633-638 (2016).
- 19. Rust, C.; Shapturenka, P.; Spari, M.; Jin, Q.; Li, H.; Bacher, A.; Guttmann, M.; Zheng, M.; Adel, T.; Hight Walker, A. R.; Fagan, J. A.; Flavel, B. S. *The Impact of Carbon Nanotube Length and Diameter on their Global Alignment by Dead-End Filtration. Small* 19, 2206774 (2022).
- 20. Walker, J. S.; Fagan, J. A.; Biacchi, A. J.; Kuehl, V. A.; Searles, T. A.; Hight Walker, A. R.; Rice, W. D. Global Alignment of Solution-Based Single-Wall Carbon Nanotube Films via Machine-Vision Controlled Filtration. Nano Lett. 19, 7256-7264 (2019).
- 21. Chiu, K.-C.; Falk, A. L.; Ho, P.-H.; Farmer, D. B.; Tulevski, G.; Lee, Y.-H.; Avouris, P.; Han, S.-J. Strong and Broadly Tunable Plasmon Resonances in Thick Films of Aligned Carbon Nanotubes. Nano Lett. 17, 5641–5645 (2017).
- 22. Hong, J. T.; Park, D. J.; Yim, J. H.; Park, J. K.; Park, J.-Y.; Lee, S.; Ahn, Y. H. Dielectric Constant Engineering of Single-Walled Carbon Nanotube Films for Metamaterials and Plasmonic Devices. J. Phys. Chem. Lett. 3950-3957 (2013).
- 23. Afinogenov, B. I.; Kopylova, D. S.; Abrashitova, K. A.; Bessonov, V. O.; Anisimov, A. S.; Dyakov, S. A.; Gippius, N. A.; Gladush, Y. G.; Fedyanin, A. A.; Nasibulin, A. G. *Midinfrared Surface Plasmons in Carbon Nanotube Plasmonic Metasurface. Phys. Rev. Appl.* **9**, 024027 (2018).
- 24. Piao, Y.; Meany, B.; Powell, L. R.; Valley, N.; Kwon, H.; Schatz, G. C.; Wang, Y. *Brightening of carbon nanotube photoluminescence through the incorporation of sp3 defects*. *Nat. Chem.*840-845 (2013).
- 25. Chen, J.-S.; Trerayapiwat, K. J.; Sun, L.; Krzyaniak, M. D.; Wasielewski, M. R.; Rajh, T.; Sharifzadeh, S.; Ma, X. Long-lived electronic spin qubits in single-walled carbon nanotubes. *Nat. Commun.* 14, 848 (2023).
- 26. McCullagh, A. M.; Gibson, E. K.; Parker, S. F.; Refson, K.; Lennon, D. *The adsorption of nitrobenzene over an alumina-supported palladium catalyst: an infrared spectroscopic study. Phys. Chem. Chem. Phys.* **25**, 25993-26005 (2023).
- 27. Clarkson, J.; Ewen Smith, W. A DFT analysis of the vibrational spectra of nitrobenzene. J. Mol. Struct. 655, 413-422 (2003).
- 28. Sebastian, F. L.; Zorn, N. F.; Settele, S.; Lindenthal, S.; Berger, F. J.; Bendel, C.; Li, H.; Flavel, B. S.; Zaumseil, J. Absolute Quantification of sp3 Defects in Semiconducting Single-Wall Carbon Nanotubes by Raman Spectroscopy. J. Phys. Chem. Lett. 13, 3542-3548 (2022).

- 29. Sykes, M. E.; Kim, M.; Wu, X.; Wiederrecht, G. P.; Peng, L.; Wang, Y.; Gosztola, D. J.; Ma, X. *Ultrafast Exciton Trapping at sp3 Quantum Defects in Carbon Nanotubes*. *ACS Nano* 13, 13264-13270 (2019).
- 30. Brown, S. D. M.; Jorio, A.; Corio, P.; Dresselhaus, M. S.; Dresselhaus, G.; Saito, R.; Kneipp, K. *Origin of the Breit-Wigner-Fano lineshape of the tangential G-band feature of metallic carbon nanotubes*. *Phys. Rev. B* **63**, 155414 (2001).
- 31. Strano, M. S.; Dyke, C. A.; Usrey, M. L.; Barone, P. W.; Allen, M. J.; Shan, H.; Kittrell, C.; Hauge, R. H.; Tour, J. M.; Smalley, R. E. *Electronic Structure Control of Single-Walled Carbon Nanotube Functionalization*. *Science* **301**, 1519-1522 (2003).
- 32. Roberts, J. A.; Yu, S. J.; Ho, P. H.; Schoeche, S.; Falk, A. L.; Fan, J. A. *Tunable Hyperbolic Metamaterials Based on Self-Assembled Carbon Nanotubes*. *Nano Lett.* **19**, 3131-3137 (2019).
- 33. S. D. M. Brown, A. Jorio, P. Corio, M. S. Dresselhaus, G. Dresselhaus, R. Saito, K. Kneipp. Origin of the Breit-Wigner-Fano lineshape of the tangential G-band feature of metallic carbon nanotubes. Phys. Rev. B 63, 155414 (2001).
- 34. Gardner, A. M.; Wright, T. G. Consistent assignment of the vibrations of monosubstituted benzenes. J. Chem. Phys. 135, 114305 (2011).
- 35. Artyukhin, A. B.; Stadermann, M.; Friddle, R. W.; Stroeve, P.; Bakajin, O.; Noy, A. *Controlled Electrostatic Gating of Carbon Nanotube FET Devices. Nano Lett.* **6**, 2080-2085 (2006).
- 36. Lerner, M. B.; Resczenski, J. M.; Amin, A.; Johnson, R. R.; Goldsmith, J. I.; Charlie Johnson, A. T. *Toward Quantifying the Electrostatic Transduction Mechanism in Carbon Nanotube Molecular Sensors. J. Am. Chem. Soc.* **134**, 14318–14321 (2012).



